To be presented at the ICCM-17 17th International Conference on Composite Materials
27 Jul 2009 - 31 Jul 2009, Edinburgh International Convention Centre (EICC), Edinburgh, UK.

FAILURE OF LIQUID-FILLED FILAMENT-WOUND COMPOSITE TUBES SUBJECTED TO AXIAL IMPACT

K. Inaba† and J.E. Shepherd‡
†Tokyo Institute of Technology, 2-12-1 Ookayama, Meguro-ku,
Tokyo, 152-8552, JAPAN, inaba@mech.titech.ac.jp
‡California Institute of Technology, 1200 E California Blvd,
Pasadena, CA 91125, USA, joseph.e.shepherd@caltech.edu

SUMMARY

We have studied the damage and rupture failure of water-filled filament-wound composite tubes due to stress waves generated by fluid-structure interaction resulting from axially-directed projectile impact on the water. Onset of the failure appears to be transverse cracking for the 45° tubes and through-lamina cracking for the 60° tubes.

Keywords: Fluid-structure interaction, Composite, Filament wound tube, Flexural wave, Failure

INTRODUCTION

The propagation of coupled fluid and solid stress waves in liquid-filled tubes serves as a model for the impact of shock waves on marine structures and is directly relevant to the common industrial problem of water hammer [1]. The main wave propagation mode is flexural wave in the structure which coupled to a pressure wave in the liquid. In our laboratory, we are examining various aspects of this problem by using projectile impact and thin-wall, water-filled tubes to generate stress waves in the water to excite flexural waves in the tube wall, see Fig. 1.

We have been using this configuration to study [2, 3] elastic and plastic waves in water-filled metal and polymer tubes. The classical theory of water hammer and our previous studies show that the extent of fluid-solid coupling for homogeneous tubes materials is determined by a non-dimensional parameter

$$\beta = \frac{2Ka}{Eh} \ , \tag{1}$$

where K is the fluid bulk modulus, E is the solid Young's modulus, a is the tube radius, and h is the wall thickness. In this case, the coupling is independent of the

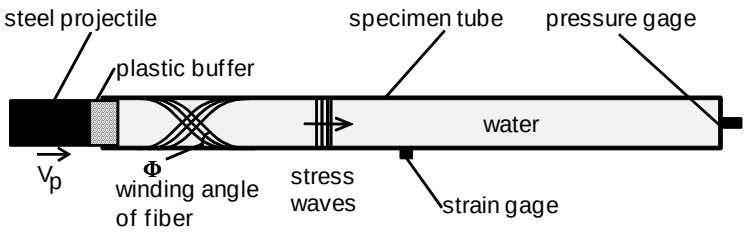

Figure 1: Schematic diagram of axi-symmetric water-in-tube configuration for generation of tube flexural waves coupled with stress waves propagating in the water.

blast wave characteristics and only depends on the fluid and solid properties and geometry. The Korteweg waves travel at a speed (Lighthill [4])

$$c = \frac{a_f}{\sqrt{1+\beta}} \,, \tag{2}$$

which, depending on the magnitude of β, can be significantly less than the sound speed a_f in the fluid or the bar wave speed $\sqrt{E/\rho_s}$ in the tube. At present, there are no published extensions of this model to composite materials so we use the classical model as a guide to interpreting our experiments with effective (mixture-averaged) values of material properties for composite tubes. The value of the effective parameter β is sufficiently large in our present experiments that we obtain significant fluid-solid coupling effects. Previous experiments in our laboratory [5] on flexural waves excited by gaseous detonation are superficially similar to the present study but these have all been in the regime of small β.

The current study reports results of high-speed impact tests that created damage or complete failure of the composite tubes. In a companion study [6], we report the results for elastic wave propagation generated by low-speed impacts. The present work extends in a systematic fashion our previous studies [2, 3] in which we used metal tubes or commercial composite tubes which were consisted of an axial fiber core with a woven cloth over-wrap and vinylester resin. In that work, we found [3] that the axial strain is a much smaller fraction (1/10) of the hoop strain than for the aluminum tubes. In the present study, we used filament wound specimen tubes so that a much larger coupling between hoop and axial motion is anticipated and also the fiber and matrix properties were better known than in the previous testing. We have interpreted our results using laminate models composite to predict effective tube modulus (hoop and axial) as a function of the fiber winding angle. Moreover, we examined the failure behavior of the composite tubes under impulsive loading.

EXPERIMENTAL METHODS

Gas gun

We designed and built an air cannon (Fig. 2) that is capable of projectile exit velocities more than 200 m/s and with a barrel diameter of 50 mm. The air cannon is mounted vertically above a specimen tube filled with water. The 1.5 kg steel

projectile is accelerated by compressed air using driver (reservoir) pressures, P_D, up to 16 MPa. The launching procedure and the details of the cannon are described in the author's paper [7].

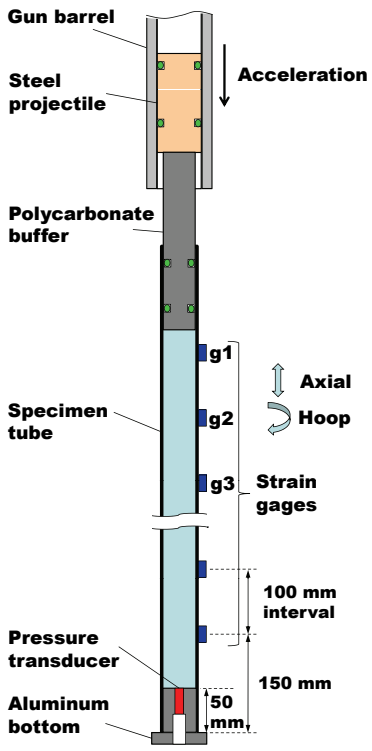

Figure 2: Schematic of test specimen tube with projectile, buffer, pressure transducer, and strain gages.

The projectile is not completely ejected from the barrel when it impacts a polycarbonate buffer placed on the water surface (see Fig. 2). A gland seal is used to prevent water moving through the clearance space between the buffer and specimen tube. In this fashion, the stress waves due to the impact of the projectile are transmitted directly to the water surface inside the specimen tube. This prevents the projectile from impacting the specimen tube directly and enables us to measure the wave velocities without interference from axial waves created by the projectile impact on the tube itself.

The impact generated stress waves in the water cause the tube to deform and the resulting coupled fluid-solid motion propagates down the tube. The deformation of the tube is measured by strain gages oriented in the hoop and longitudinal directions and the pressure in the water is measured by a piezoelectric transducer (Fig. 2) mounted in an aluminum fitting sealed to the bottom of the tube. The bottom of the tube is fastened to an aluminum bar mounted in a lathe chuck that is placed directly on the floor. The top and bottom of the tube were reinforced with a circumferential clamp to prevent radial expansion and fluid leakage.

Table 1: Test Matrix.

shot	tube	winding angle $\pm\Phi$ [deg]	wall-thickness [mm]	inner diameter [mm]	buffer speed [m/s]
067	CFRP#7	45*	1.74	38.3	47.5
071	CFRP#8	60	1.65	38.3	37.5
076	CFRP#4-1	45	1.66	38.3	37.5
105	CFRP#5-1	45	1.59	38.3	40.8
107	CFRP#9	60	1.65	38.3	43.9
109	CFRP#6-1	45	1.74	38.3	40.8
111	CFRP#5-2	45	1.74	38.3	35.7
114	GFRP#3	50	1.60	38.8	35.7

*Roll-wrapped sheet, ply angle

Materials and methods

We examined in our tests two types of specimens constructed either with glass-fiber reinforced plastic (GFRP) or carbon-fiber reinforced plastic (CFRP) construction with three winding angles. Nominal wall-thickness and inner diameter are listed in the Table 1. The length of all specimen tubes was 0.9 m. Shot 067 was carried out using a specimen tube consisting of roll-wrapped CFRP sheets. Shots 071 and 107 were carried out with a CFRP tube which has a winding angle of 60° and woven pattern I as shown in Fig. 3. All CFRP tubes were fabricated from HTS 5631-12K carbon fibers and thermosetting epoxy matrix resin (UF3325). Each tube was made up of three plies with a lay-up sequence of $+\Phi - \Phi + \Phi$ where Φ is the winding angle. Shots 076 and 105, 111 and 109 were conducted with specimens of 45° winding angle and woven patterns I, II, or III. Depending on the pattern, the wall-thickness varies: pattern I, 1.66 mm; pattern II, 1.59 mm, pattern III, 1.74 mm. Finally, Shot 114 was performed with a GFRP tube, winding angle of 50°.

Each test specimen is instrumented at 100 mm increments with 12–14 strain gauges for measuring hoop and axial strains. A single piezoelectric pressure transducer recorded the pressure wave reflected from the aluminum plug at the bottom of the specimen. A high-speed video camera is used to observe the buffer motion due to the projectile impact and determine the buffer speeds by post-processing the images.

RESULTS AND DISCUSSION

Primary wave speeds and reflected pressures

Figure 4 shows hoop and axial strain histories measured at locations g1 (bottom trace) to g6 as presented in Fig. 2. The top trace in Fig. 4a is the pressure history and since this is obtained in the solid end wall, the pressure values are enhanced over those for the propagating wave due to the effects of reflection at the aluminum-water interface. In Fig. 4, the strain signal baselines are offset proportional to the distance between the gages so that we can also interpret the trajectories of signal features

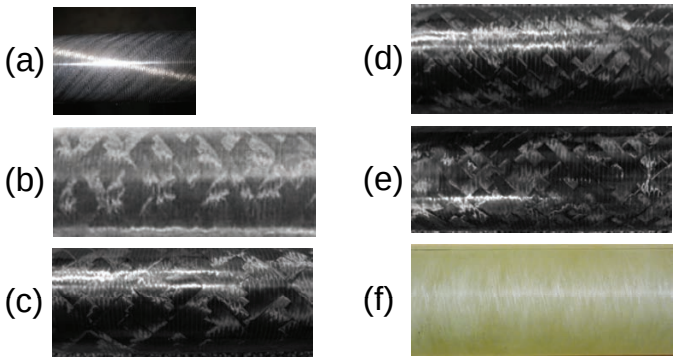

Figure 3: Test specimen tubes (a) CFRP#7, roll-wrapped sheet with ply angle of 45°, (b) CFRP#8,9, $\Phi = 60°$, pattern I, (c) CFRP#4-1, $\Phi = 45°$, pattern I, (d) CFRP#5-1,2, $\Phi = 45°$, pattern II, (e) CFRP#6-1, $\Phi = 45°$, pattern III, (f) GFRP#3, $\Phi = 50°$.

by considering the ordinate as a space location as well as a signal amplitude. The lines labeled 3586 m/s and 663 m/s indicate the leading edge of the precursor wave and the primary (main) stress wave fronts, respectively. Although the wall-thickness slightly varies for each woven pattern, the wall-thickness variations within patterns I to III are too small to result in noticeable differences in wave speed. The wave speeds obtained in shot 105 with a buffer speed of 40.8 m/s just after the projectile impact are similar to the wave speeds at lower buffer speeds of 5.3 m/s [6]. The maximum reflected pressure is 23.0 MPa , which is 2–3 times larger than previous results with lower buffer speeds.

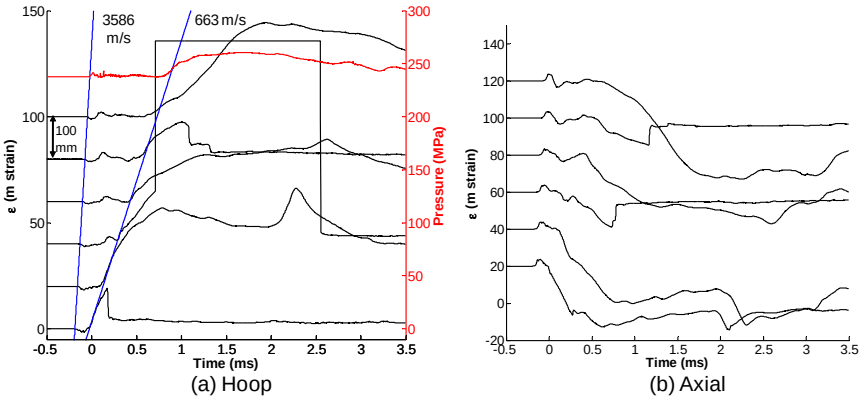

Figure 4: Strain and pressure histories for shot 105, CFRP 45° tube, wall-thickness 1.66 mm, pattern I.

Comparing with the tube of 45° winding angle, the 60° tube has a shorter pitch of the fiber strands and thus is stronger in hoop direction. The precursor wave and the primary wave propagate at 2862 m/s and 1059 m/s, respectively, with an initial buffer speed of 43.9 m/s. The precursor wave of the 60° tube is slower and the

primary wave faster than those of the 45° tube. Although the specimen tubes burst for high-speed impact, the relation between wave speeds and winding angle is in a good agreement with those at lower speeds [6]. The maximum reflected pressure reaches 83.1 MPa and is much larger than that for the tube with a 45° winding angle. At lower-buffer speeds, there was no clear dependence of the reflected pressures on the winding angle [6].

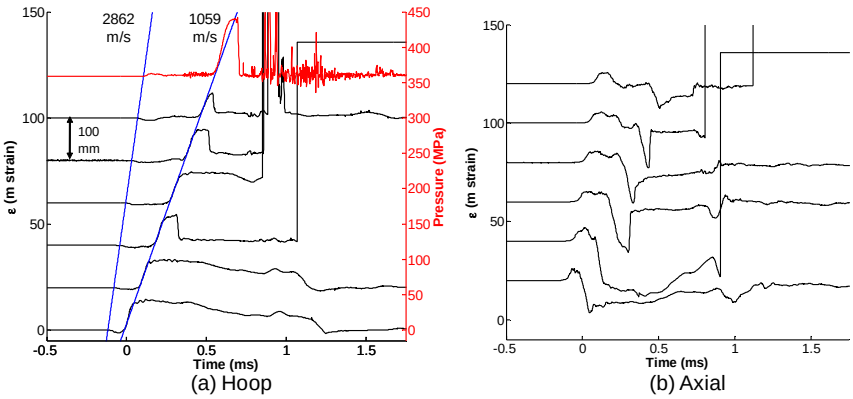

Figure 5: Strain and pressure histories for shot 107, CFRP 60° tube, wall-thickness 1.65 mm, pattern I.

Shot 114 was conducted with the GFRP tube which has a winding angle of 50°. Figure 6 shows hoop and axial strain histories in shot 114. Precursor and primary wave velocities measured for the axial and hoop wave fronts are 2581 m/s and 971 m/s. Since the fiber and matrix properties, particularly the volume loading of fibers, are obviously different for the GFRP and CFRP specimens, the results for the GFRP tube are inconsistent with the CFRP tube. The peak of the reflected pressure is 79.3 MPa, similar that measured for the CFRP tubes.

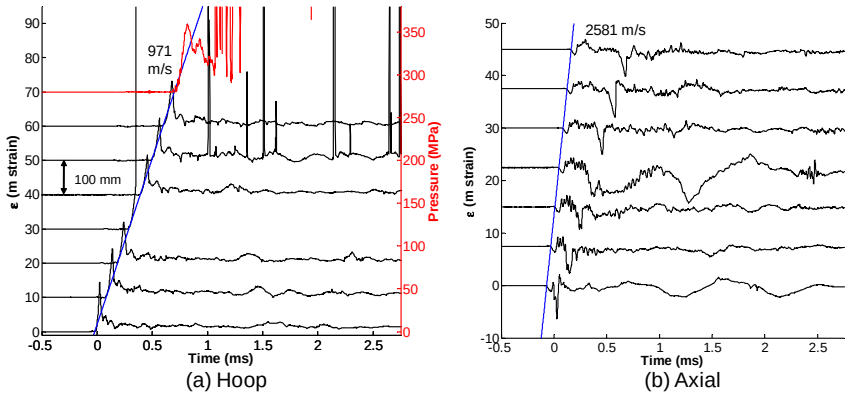

Figure 6: Strain and pressure histories for shot 114, GFRP 50° tube, wall-thickness 1.60 mm, helical winding.

Effective Young's modulus and Wave Speeds

In order to interpret the results of our experiments using the classical Korteweg model, we need to estimate the effective Young's modulus of the composite materials. We have done this using two versions of the laminate theory of effective modulus. The first estimate is based on the models developed by Puck and Schneider [8] for fiber-reinforced plastics; the models are reviewed by Greenwood [9] and utilized by Hull, Legg and Spencer [10], Spencer and Hull [11] and Hull and Clyne [12]. Puck's analysis supposes that the resin has zero strength and modulus. The second estimate is based on the general two-dimensional elastic theory of laminae as described by Hull and Clyne [12]; this includes the strength and modulus of the resin as well as the fibers. Each laminae is assumed to be in a state of plane stress in order to compute the off-axis components of the compliance matrix.

Figure 7 shows the wave speeds and Young's modulus derived from Puck's analysis (a,b) and from the 2-D off-axis analysis (c,d). The bar speed $\sqrt{E_a/\overline{\rho}}$ was used as an estimate of the precursor wave speed where E_a is the tube modulus in the axial direction and $\overline{\rho}$ is the average density of the composite. The primary wave speed is estimated using the Korteweg speed (Eq. 2) based on a value of β (Eq. 1) obtained from the modulus E_h in the hoop direction. The observed wave speeds and the Korteweg model are used to estimate the effective hoop modulus shown in Figs. 7b and d. Property data listed in Table 2 were used to estimate E_a and E_h from the models [6].

Despite very approximate nature of our estimates, we find reasonable agreement for wave speeds (see Fig. 7a,c) using either model. The general 2-D theory including the resin modulus gives a better estimation of the transverse modulus (see Fig. 7b,d) than does the simpler Puck theory. Since the main damage mechanism in the present situation is associated with the primary wave, we adopted the general 2-D off-axis analysis to estimate the strength of the tube in analyzing the failure mechanisms. To make further progress, it will be necessary to analyze the problem with more realistic model of fluid-structure coupling to composites.[1]

Similar estimates can be made for the GFRP tube and we have determined that the effective Young's modulus for the hoop direction is about 40.1 GPa in the present (plastic) case. This is about 34% higher than the elastic value of 30.0 GPa [6] and 45% higher than the nominal value of 27.6 GPa given by Watters [14]. It is not clear why the models do not work as well for the GFRP as for the CFRP for the plastic case.

Failure Mechanisms and Strength Estimates

To understand the observed failure mechanisms and tube strength, we have performed some estimates of the composite tube strength. In doing so, we have followed the methods presented in Chapter 8 of Hull and Clyne [12]. For example, an idealized stress-strain behavior for loading a single CFRP laminae in the fiber direction is shown in Fig. 8. The composite properties listed in the Table 2 indicate that the

[1] Jeong Ho You and Kauschik Bhattacharya of CIT have recently developed [13] a theoretical treatment that extends the four-equation model of water hammer by computing the elastic properties of the composite tube using a standard laminate model of the composite material.

Table 2: Material properties of CFRP tube.

Fiber		
Young's modulus	E_f	238 GPa
Density	ρ_f	1770 kg/m^3
Poisson's ratio*	ν_f	0.3
Elongation at Break	ϵ_{fu}	1.8 %
Tensile strength	σ_{fu}	4620 MPa
Matrix		
Tensile modulus	E_m	2.83 GPa
Density	ρ_m	1208 kg/m^3
Tensile Poisson's ratio*	ν_m	0.280
Elongation at Break	ϵ_{mu}	5.5 %
Tensile strength	σ_{mu}	68.95 MPa
Composite		
Volume fraction of fiber	V_f	0.7

*Data from Hull and Clyne [12]

matrix has the larger failure strain ($\epsilon_{mu} > \epsilon_{fu}$). If matrix fracture takes place while the fibers are still bearing some load, as shown in Fig. 8, then the composite failure stress σ_{1u} parallel to the fibers is

$$\sigma_{1u} = V_f \sigma_{fu} + (1 - V_f)\sigma_{mfu} \ , \tag{3}$$

where σ_{mfu} is the matrix stress at the onset of fiber cracking. The tensile strength σ_{1u} of the CFRP material computed on this basis is 3014 MPa.

Tensile failure transverse to the fiber direction is more complex as discussed by Hull and Clyne [12]. An estimate of the effect of the presence of the fibers on the transverse strength can be obtained by treating the fibers in the composite as a set of cylindrical holes and considering the reduction in load-bearing cross-section. This estimation is not accurate but useful as a guide. The transverse failure strain estimated using this idea is

$$\sigma_{2u} = \sigma_{mu} \left[1 - 2 \left(\frac{V_f}{\pi} \right)^{1/2} \right] \ . \tag{4}$$

The estimated transverse strength σ_{2u} is 3.86 MPa, much smaller than σ_{1u}. The shear strength can be estimated by the HMH (Huber-v.Mises-Hencky) criterion [8], which relates the shear strength to tensile strength by

$$\tau_{12u} = \frac{1}{\sqrt{3}} \sigma_{mu} \ . \tag{5}$$

Evaluating this expression for CFRP, we obtain $\tau_{12u} = 39.8$ MPa.

A number of failure criteria have been proposed and examined for the static situation; the maximum stress criterion [12], the maximum strain criterion, and the combined-stress criterion such as those of Tsai and Wu [15] and Christensen [16].

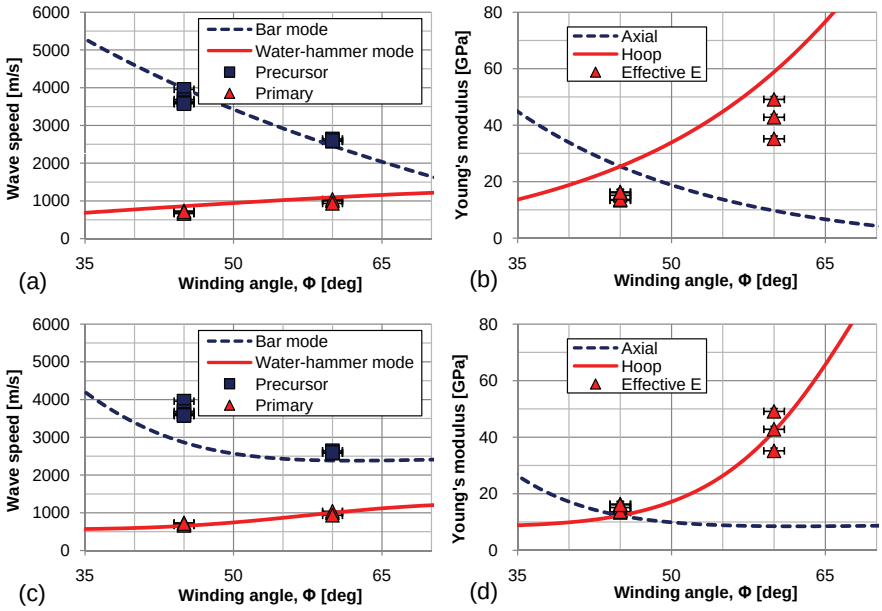

Figure 7: Predicted and experimental dependence of primary and precursor wave speeds on the winding angle for (a) Puck's analysis and (c) 2-D off-axis analysis. Predicted and effective Young's modulus dependence on winding angle for (b) Puck's analysis and (d) 2-D off-axis analysis.

As the first step for studying on the failure due to dynamic loading, we have applied the maximum stress analysis. The maximum stresses in the component plies were calculated assuming pure hoop loading without any axial component. The failure stresses predicted by the maximum stress criterion based on σ_{1u}, σ_{2u} and τ_{12u} are plotted in Fig. 9 as a function of winding angle Φ for CFRP tubes. The shear stress in the second ply has the opposite sign to the other two plies in Fig. 9a while there is no difference between plies in the stresses parallel and normal to fibers. The predicted failure stresses of the tube with the winding angles at 45° and 60° are 55.1 MPa (transverse failure) and 223 MPa (shear failure), respectively.

Failure Observations

In shot 105, we recorded a movie of the buffer motion and the failure at the top portion of a CFRP tube. Figure 10 shows a series of frames from the high-speed video between -690 μs to 3510 μs, corresponding to the time range shown in Fig. 4. The interval between images is 350 μs. After the impact at -690 μs, the specimen tube started to deform due to the internal pressure increasing, and a bulge developed near the buffer bottom surface. Between the 3rd and the 4th frames (10–360 μs), some fibers broke on the right side of the bulge. Between the 7th and the 8th frames (1760–2110 μs), the tube burst on the left side of the bulge and water spouted from the failure region. Comparison of the strain and video images, indicates that the initial fiber failure occurred shortly after the impact and the tube burst occurred after the reflected wave from the bottom end arrived at around the 6th frame when

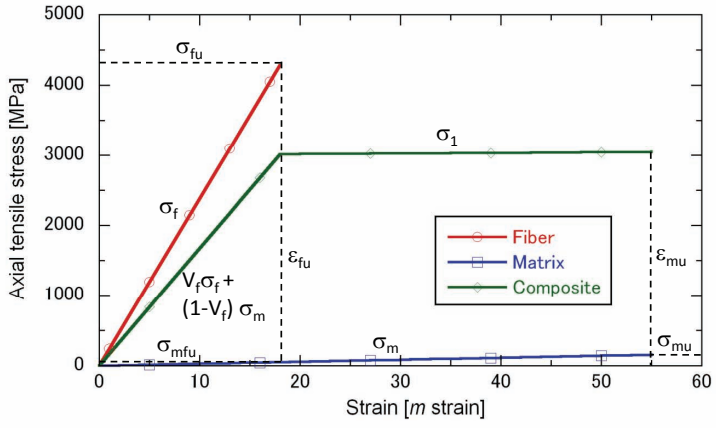

Figure 8: Idealized tensile stress-strain plots for fiber, matrix and composite in case of CFRP laminae with loading parallel to the fibers.

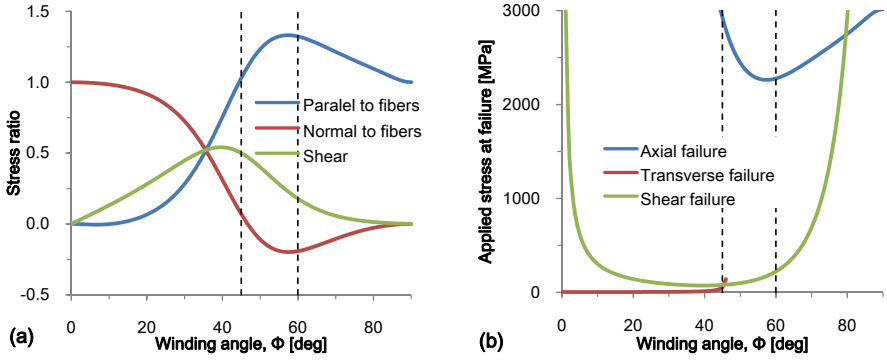

Figure 9: Calculated variations of (a) the internal stresses, relative to an applied tensile stress and (b) the applied stress needed to cause different types of failure, as a function of the winding angle Φ for an laminate of CFRP tube.

water spouted from the top of the tube.

The strain and reflected pressure histories are shown in Fig. 4. In some cases, the strain gages remained intact and indicated more than 37 *m*strain due to the primary wave. Rotem and Hashin [17] reported that for ply angles close to ±45° the material behavior can be classified as ductile (large elongation) while at the other angles the behavior resembles brittle material. The bulge created immediately after the impact resembles the ductile bulge observed in our experiments on the plastic deformation of mild steel tubes [7].

Photographs of several tube failures are shown in Figure 11. Figures 11a and c show the rupture of the CFRP tube at the top of the specimen with the roll-wrapped 45° sheets and the winding angle of 45°, respectively. Fibers were torn and large-scale damage can be seen. Even though the 45° tube did not burst, we observe white streaks parallel to the fiber direction (see Fig. 11b). The white streaks are known to be the first signs of visible damage as discussed by Jones and Hull [18], who also observed that rupture was associated with bending and delamination on

Figure 10: Series of frames from high-speed video showing the burst of the CFRP tube near the buffer bottom surface after the projectile impact in shot 105. The interval between images is 350 μs (-690 μs to 3510 μs in Fig. 4).

the compressive side of the bend. This agrees with our observations in shot 105 as shown in Fig. 10. The 60° CFRP tube and the 50° GFRP tube burst at the bottom end of the tube (see Fig. 11d,e). We have no images of the bottom portion of the tube and can only speculate what happened to the specimen from the strain and reflected pressure histories. After the testing, the bottom end of the 60° CFRP tube was found to be cut by the circumferential clamp; this is the reason why the failure edges are relatively straight. The 50° GFRP tube burst in a fashion similar to the static failure observed by Hull *et al.* [10]. In shot 114 with the GFRP tube, we observed a cloud or spray of water ejected through cracks in the tube at the top part of the specimen near the lower end of the buffer. After the experiment, we were able to detect deep streaks parallel to the fibers near the location where the water spray was observed.

The predicted failure stresses of CFRP tubes with 45° and 60° winding angles are 55.1 MPa for transverse failure and 223 MPa for through-lamina shear failure, respectively. Internal pressures, P_{int}, calculated from the reflected pressure by the P-u diagram method [7] are 10–15 MPa for the 45° cases and 40–45 MPa for the 60° cases. The hoop stress ($\sigma_H = P_{int}a/h$) for the 45° case is 140–180 MPa, is larger than the minimum failure stress for transverse failure and approaching that for shear failure. It is likely that the onset of transverse cracking (lamina cracking) always occurred in 45° cases.

Rotem and Hashin [17] indicated that the onset of failure of the 60° tube is not due to transverse failure, but to interlaminar shear stress at the edges. They considered that the interlaminar delamination does not affect the apparent load and elongation, as long as the laminae themselves do not fail. When through-lamina cracking starts, the specimen fails instantaneously. The large interlaminar shear is also obtained by the finite-difference simulation of Pipes and Pagano [19]. Hoop stress σ_H for 60° cases is 460–560 MPa and larger than the through-lamina shear failure stress (223 MPa). Therefore, not only interlaminar delamination but also through-lamina cracking is expected to occur for 60° cases. In shots 067, 105, 107

and 114, complete fracture (fiber failure) occurred. The failure stresses of the fiber plotted in Fig. 9 are 2928 MPa and 2278 MPa for 45° and 60° tubes, respectively. Using the reflected pressure, the maximum hoop stress is calculated to be 1000 MPa for 60° tubes and half of the failure stress of the fiber. Possible reasons for the complete failure of the fiber are: additional force due to the off-axis impact of the buffer, axial loading effects, dynamic loading effects, and local stress concentrations. Further analysis is needed to understand the true origin of complete failure in these cases.

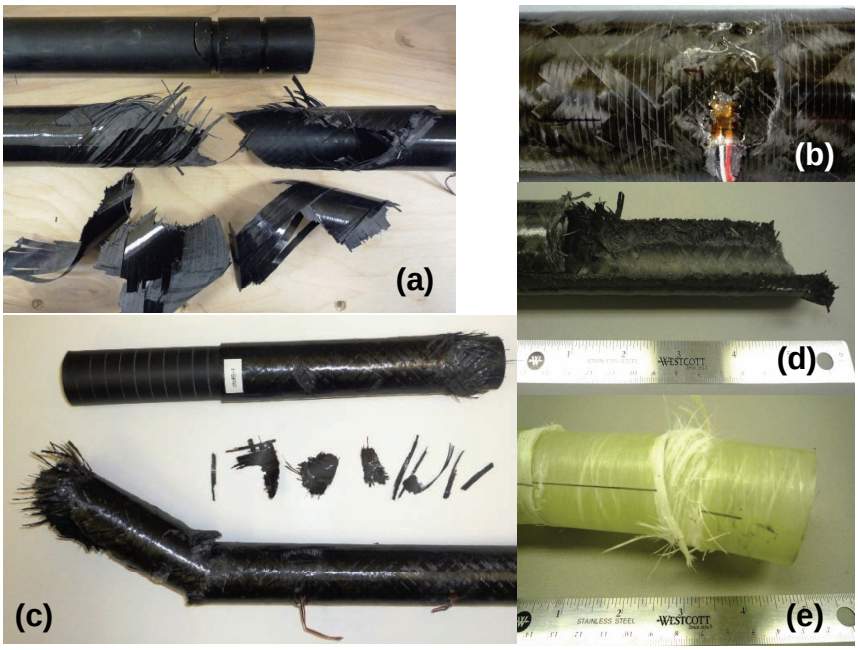

Figure 11: Post-test photographs of the failure regions for (a) burst at the top of roll-wrapped CFRP (45°) in shot 067, (b) damage (fine white streaks parallel to the fibers) on the side of CFRP (45°) in shot 076, (c) burst at the top of CFRP (45°) in shot 105, (d) burst at the bottom of CFRP (60°) in shot 107, (e) burst at the bottom of GFRP (60°) in shot 114.

CONCLUSION

We have shown that the construction and materials of filament-wound composite tubes have a significant effect on wave propagation and failure processes in water-hammer type response of liquid-filled tubes. Using simple models for the effective modulus of the tube, we have shown that the main flexural wave disturbance travels at a Korteweg speed that is consistent with the effective modulus for the hoop direction of deformation for both CFRP and GFRP tubes. The precursor waves travel at a speed close to the bar speed based on the effective modulus for the axial direction. The dependence of the wave speed with winding angle is in reasonable agreement for the limited range of angles that we have examined. Onset of failure appears to be due to transverse cracking for 45° tubes and through-lamina cracking

for the 60° tubes. The failure mechanism of the CFRP tube wound at 45° is ductile-like while at 60° the behavior is brittle-like. The estimated stresses for the onset of failure are consistent with conventional failure criteria although no effort was made to determine the actual failure thresholds. Complete failure of the fibers and matrix were observed in some cases with peak hoop stresses estimated to be a factor of two lower than the fiber tensile strength.

ACKNOWLEDGEMENTS

This research was sponsored by the Office of Naval Research, DOD MURI on Mechanics and Mechanisms of Impulse Loading, Damage and Failure of Marine Structures and Materials (ONR Grant No. N00014-06-1-0730), program manager Dr. Y. D. S. Rajapakse. We thank Tomohiro Nishiyama of Japan Patent Office for his help in conducting the experiments and Prof. G. Ravichandran for his support and advice.

References

[1] Wiggert, D. C., and Tijsseling, A. S., 2001. "Fluid transients and fluid-structure interaction in flexible liquid-filled piping". *Applied Mechanics Reviews,* **54**(5), pp. 455–481.

[2] Inaba, K., and Shepherd, J. E., 2008. "Flexural waves in fluid-filled tubes subject to axial impact". In Proceedings of the ASME Pressure Vessels and Piping Conference. July 27-31, Chicago, IL USA. PVP2008-61672.

[3] Inaba, K., and Shepherd, J. E., 2008. "Impact generated stress waves and coupled fluid-structure responses". In Proceedings of the SEM XI International Congress & Exposition on Experimental and Applied Mechanics. June 2-5, Orlando, FL USA. Paper 136.

[4] Lighthill, J., 1978. *Waves in Fluids.* Cambridge University Press.

[5] Shepherd, J. E., 2009. "Structural response of piping to internal gas detonation". *Journal of Pressure Vessel Technology,* **131**(3). in press.

[6] Inaba, K., and Shepherd, J. E., 2009. "Fluid-structure interaction in liquid-filled composite tubes under impulsive loading". In Proceedings of the 2009 SEM Annual Conference & Exposition on Experimental and Applied Mechanics. June 1-4, Albuquerque, New Mexico USA.

[7] Inaba, K., and Shepherd, J. E., 2009. "Plastic deformation and vibration in a fluid-filled tube subject to axial impact". In Proceedings of the ASME Pressure Vessels and Piping Conference. July 26-30, Prague, Czech Republic. PVP2009-77821.

[8] Puck, A., and Schneider, W., 1969. "On failure mechanisms and failure criteria of filament-wound glass-fibre/resin composites". *Plastic and Polymers,* **37**, pp. 33–44.

[9] Greenwood, R., 1977. "German work on GRP design". *Composites,* **7**, pp. 175–184.

[10] Hull, D., Legg, M., and Spencer, B., 1978. "Failure of glass/polyester filament wound pipe". *Composites,* **9**, pp. 17–24.

[11] Spencer, B., and Hull, D., 1978. "Effect of winding angle on the failure of filament wound pipe". *Composites,* **9**, pp. 263–271.

[12] Hull, D., and Clyne, T., 1996. *An Introduction to Composite Materials*, 2nd ed. Cambridge University Press.

[13] You, J. H., and Bhattacharya, K., 2009. California Institute of Technology, personal communication. January.

[14] Watters, G. Z., 1984. *Analysis and Control of Unsteady Flow in Pipelines.* Butterworth Publishers, MA.

[15] Tsai, S., and Wu, E., 1971. "A general theory of strength for anisotropic materials". *J. Composite Materials,* **5**, pp. 58–80.

[16] Christensen, R., 1979. *Mechanics of Composite Materials.* Dover.

[17] Rotem, A., and Hashin, Z., 1975. "Failure modes of angle ply laminates". *J. Composite Materials,* **9**, pp. 191–206.

[18] Jones, M., and Hull, D., 1979. "Microscopy of failure mechanisms in filament-wound pipe". *J. Materials Science,* **14**, pp. 165–174.

[19] Pipes, R., and Pagano, N., 1970. "Interlaminar stresses in composite laminates under uniform axial extension". *J. Composite Materials,* **4**, pp. 538–552.